

Excitation of multiple resonances in 1D Anderson localized systems for efficient light amplification

Seung Ho Choi,¹ Kyung Min Byun,² and Young L. Kim^{1,2,*}

¹Weldon School of Biomedical Engineering, Purdue University, West Lafayette, Indiana 47907, USA

²Department of Biomedical Engineering, Kyung Hee University, Yongin 446-701, South Korea

*Corresponding author: youngkim@purdue.edu

Received December 18, 2014; revised January 23, 2015; accepted January 24, 2015;
posted January 28, 2015 (Doc. ID 230970); published February 27, 2015

Excitation of hybridized multiple resonances can be an effective route for coherent light generation in irregular 1D systems larger than the localization length of light. Necklace states are often considered to have nonlocalized states. However, we propose that some hybridized/coupled states can have high-resonant tunneling with spatially extended fields. If strong localization properties are preserved in hybridized resonances, the excitation of such states allows for deposition of the excitation energy deep into the structure and spatial overlap with local gain regions. This result could allow for better utilizing hybridized resonances in biological or natural photonic systems. © 2015 Optical Society of America

OCIS codes: (140.3410) Laser resonators; (290.4210) Multiple scattering; (140.2050) Dye lasers; (140.4780) Optical resonators; (240.7040) Tunneling; (230.4170) Multilayers.

<http://dx.doi.org/10.1364/OL.40.000847>

Light transport through resonances or modes in irregular and open media has been the subject of intensive investigation to capitalize on partially disordered photonic structures. Multiple resonances in low-dimensional disordered photonic structures can be coupled to form hybridized states that are overlapped in space as well as frequency [1,2]. These hybridized states are known as necklace states, because a collection of such modes generates a long chain with multiple peaks in space [1]. Necklace states are often considered nonlocalized states, while dominating the transmission statistics due to relatively broad spectral bandwidths [3]. Recently, the concept of necklace states has been extended to include superposition of quasi-modes with several narrow peaks in transmission spectra [4–8]. Such hybridized states are also called extended quasi-modes or short necklace states. Therefore, hybridized states can be classified into two cases, using the degree of local spectral mode overlap: (i) When the mode spacing $\Delta\omega < \delta\omega$, hybridized states are spatially extended with relatively broadened spectral linewidths (short-lived modes), because of their short life time due to weak mode splitting. This case is the classical necklace states. (ii) When $\Delta\omega \geq \delta\omega$, hybridized states have multiple narrow peaks in transmission spectra (long-lived modes), and similar multiple peaks in space are extended [4–8]. This latter has lifetimes shorter yet comparable to single localized modes, and $\delta\omega$ of the adjacent peaks is still narrow with low valleys. This hybridization is hereinafter referred to as hybridized localized states (HLS).

In this Letter, we propose that HLS can be highly beneficial for coherent light generation in disordered photonic structures in the Anderson localization regime. One major limitation in random lasers is that they require high excitation power and have low-energy conversion efficiency, hampering their practical applications. To overcome this limitation, photon localization lasers were demonstrated using a random system composed of multiple dielectric layers with interspersed gain [9]. Enhanced

light transport of localized modes resulted in low-threshold lasers. Typically, if the system size L is comparable to the localization length ξ (i.e., $L \sim \xi$), a low lasing threshold is achieved, when the excitation intensity is deposited near the center of the sample via localized modes [10,11]. As L increases while keeping ξ the same, the excitation light can dwell exponentially long inside the system, which in turn can enhance lasing performance. Given the different wave transport nature in systems with $L \gg \xi$, the previous understanding on random lasing systems, which are based on systems with $L \sim \xi$, needs to be revisited. Since gain regions are deeply located in such a large system, it would be beneficial if the excitation energy can be extended spatially. As illustrated in Fig. 1(a), a large spatial overlap between the excitation and emission fields (yellow curve) is allowed, if the excitation energy is coupled with resonant tunneling to be deposited deep into the structure (green curve). In recent studies, highly multilayered structures are commonly found in nature [7,12], which have led to a variety of biomimetic fabrication approaches. For examples, the overall thickness of nacre (also known as mother-of-pearls) from natural pearls and abalone shells is much longer than ξ . Thus, a clear understanding of HLS of waves in large samples with $L \gg \xi$ is of particular importance.

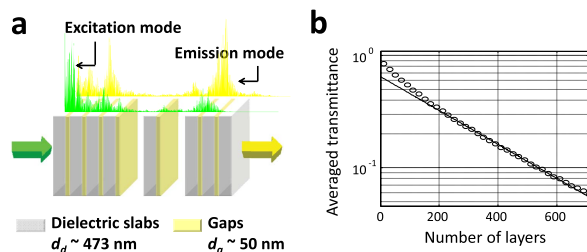


Fig. 1. (a) Schematic illustration of alternating dielectric and gap (gain for lasing modes) layers with longitudinal optical excitation. (b) Averaged transmittance as a function of the number of dielectric layers.

First, we calculated quasi-modes (i.e., in the absence of gain) to study interplay between field spatial profiles and transmission. By mimicking nacre nanostructures founded in pearls or abalone seashells [7], the transfer matrix method [7,13] was used for absorption-free dielectric multilayered samples with $L \gg \xi$. As shown in Fig. 1(b), a 2000-layered system with a total thickness of 0.5 mm was simulated with alternating high-refractive-index dielectric layers ($n_a \sim 1.65\text{--}1.67$) and lower-refractive-index gaps ($\text{Re}(n_g) \sim 1.32\text{--}1.37$). Disorder was applied by imposing variations in the layer thickness, which was determined from abalone nacre specimens by using confocal and scanning electron microscopy measurements in our previous study [7]. The thickness d_g of the gaps varied from 10 to 50 nm with a mean value of 40 nm, and the alternating layer thickness d_d was 473 nm. These structural variations resulted in $\xi \sim 73.8 \mu\text{m}$ ($L/\xi \sim 6.7$) such that $\langle \ln T \rangle \sim -L/\xi$ with the transmission T [Fig. 1(b)].

We analyzed spatial characteristics (i.e., spread and central position) of transmission field intensity and T in hybridized states in the Anderson localized regime. Previously, a ratio of T to the stored energy was successfully used as a quantitative parameter of light transport [14]. In our analyses, we focused on the spatial parameters that better capture the relationship between the field shape and the behavior of T , using an inverse participation length IPL and a centroid C_z defined such that:

$$\text{IPL} = \int I^2(z) dz / \left(\int I(z) dz \right)^2 \quad \text{and} \\ C_z = \int z I(z) dz / \int I(z) dz, \quad (1)$$

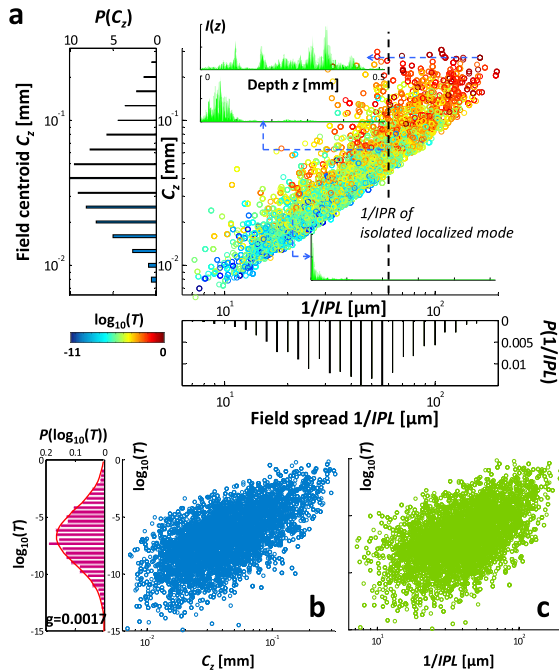


Fig. 2. (a) Distributions of the spread $1/\text{IPR}$ and central position C_z of the field intensity $I(z)$ and the transmission T (color of circle) in passive modes. (b) and (c) T as a function of $1/\text{IPR}$ and central position C_z , separately. The solid red curve is a Gaussian fit of the probability of T in a logarithmic scale $P(\log_{10}(T))$.

where $I(z)$ is the field intensity along the depth z at a wavelength $\lambda = 532 \text{ nm}$. $1/\text{IPL}$ captures the spread of the wave function. After analyzing the field patterns of 10^4 passive random configurations, we found that the field spread $1/\text{IPL}$ is proportional to the central field position C_z on a logarithmic scale, as shown in Fig. 2(a). As the wave functions are spread, C_z is shifted such that more energy is stored near the exit location of the sample. Specifically, Figs. 2(b) and 2(c) show that both increases in $1/\text{IPL}$ and C_z contribute to enhanced T . It should also be noted that the waves in the simulated structures are deeply localized, since $L/\xi \sim 6.7$. This is supported by the transmission probability statistics $P(\log_{10}(T))$, in which both low and high transmission distributions fit well with a Gaussian function [15] [red solid line of Fig. 2(b)], and a small value of the dimensionless conductance $g = \langle T \rangle = 0.002 \ll 1$. As shown in the representative transmission fields [insets in Fig. 2(a)], the nonresonant field profile corresponds to low values of $1/\text{IPL}$ and C_z . The typical isolated localized modes do not result in high T . On the other hand, when the values of $1/\text{IPL}$ and C_z are high, the transmission field is extended spatially with multiple peaks [insets in Fig. 2(a)].

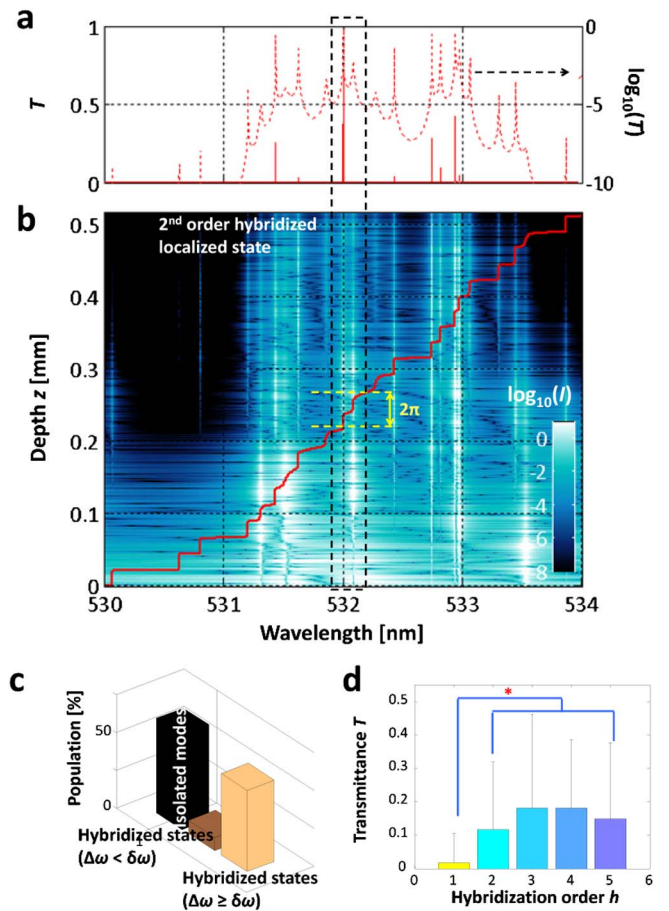


Fig. 3. Representative transmission spectra (a) and internal field (b) of HLS. (c) Occurrence populations of the isolated localized modes, the conventional necklace states ($\Delta\omega < \delta\omega$), and HLS ($\Delta\omega \geq \delta\omega$). (d) Statistical characteristics of T of different h . $h = 1$ is the isolated mode, and $h \geq 2$ are the hybridized states. The error bars are standard deviations.

We quantified the occurrence probabilities of the isolated localized modes, the conventional necklace states (i.e., $\Delta\omega < \delta\omega$), and HLS (i.e., $\Delta\omega \geq \delta\omega$) from 546 spectral peaks. We also counted the order h of HLS (i.e., number of hybridized resonances). Because the phase changes rapidly at the locations of resonances in 1D, h can be determined by the accumulated phase shift [white solid line in Fig. 3(b)] [16] and the relative height of valleys in $\log_{10}(T)$ [5]. As shown in an example of $I(z)$ and T (Fig. 3), two modes around $\lambda = 532$ nm form the second-order HLS. These spectrally adjacent states have spatially extended fields with very similar shapes [Figs. 3(a) and 3(b)]. Figure 3(c) shows that 50% of the peaks are the isolated localized modes, and 43% originate from HLS ($\Delta\omega \geq \delta\omega$). In the current system with $L \gg \xi$, the conventional necklace states ($\Delta\omega < \delta\omega$) are not as frequent as the other cases. In Fig. 3(d), T of the hybridized states is significantly higher than T of the isolated modes. Although T in the classical necklace states is not always high, the hybridized states allow for high-resonant tunneling and spatially extended fields (Fig. 2).

Second, we conducted lasing mode simulations (i.e., in the presence of gain) to investigate how the spatially extended hybridized resonances play a role in light amplification and lasing. To vary the spatial profile of excitation via HLS, the spatial distribution of the refractive index in the gain area $n_g(z, k)$ was modulated, and n_g was described by a frequency-dependent susceptibility χ_g [17]:

$$n_g(z, k) = \sqrt{n_{g(nr)}^2(z, k) + \chi_g(z, k)},$$

$$\chi_g(z, k) = \frac{A_m N_{\text{ex}}(z)}{k_a^2 - k^2 - ik\Delta k_a}, \quad (2)$$

where $n_{g(nr)}$ is the refractive index of the nonresonant background material, z is the spatial coordinate, A_m is a material-dependent constant, and N_{ex} is the spatially dependent density of excited atoms. For laser dye of Rhodamine 6G, the peak frequency of emission k_a and its spectral width Δk_a were set to be $11.38 \mu\text{m}^{-1}$ and

$0.72 \mu\text{m}^{-1}$, respectively [7]: Then, the spatially modulated N_{ex} was implemented as follows:

$$N_{\text{ex}}(z) = N_0 \times I_{\text{ex}}(z)/\Xi \quad \text{and} \quad \Xi = \int_0^L \frac{\varepsilon(z)I_{\text{ex}}(z)}{2} dz, \quad (3)$$

where N_0 is the total amount of excited atoms within the system, I_{ex} is the field intensity, and Ξ is the energy stored inside the medium. The field intensity was normalized to Ξ to account for the same N_0 in different excitation spatial profiles. Thus, this excluded possible confounding effects of different amounts of the total energy on random lasing. To use a predefined order of hybridization h , the intensity patterns of the excitation mode I_{ex} were modeled as follows [16]:

$$I_{\text{ex}}(z) = \delta(h) \exp\left(-\frac{|z|}{\xi}\right) + \sum_{i=1}^h \exp\left(-\frac{|z - z_i|}{\xi}\right), \quad (4)$$

where z_i is the position of i th peak in HLS with h (each peak is equally spaced) and δ stands for a Dirac delta function. The lifetimes (i.e., $\delta\omega$) of excitation modes were assumed to be identical under different orders of hybridization. For typical random lasers, the excitation light at a single wavelength is illuminated on the sample. Then, narrow stimulated emission peaks emerge within the broad spontaneous emission spectrum as the excitation energy increases. Thus, one can understand that the excitation mode selects lasing modes in which their emission field profiles have preferable shapes for easy activation.

As shown in Figs. 4(a) and 4(b) (left curves in the lower panels), after exerting the excitation profiles of $N_{\text{ex}}(z)$: a nonresonant mode ($h = 0$) and an isolated localized mode ($h = 1$), we evaluated evolution of lasing modes and lasing performance (i.e., lasing threshold and emission intensity). In the excitation-spectral domain [upper panels of Figs. 4(a) and 4(b)], 20 lasing modes were tracked in the spectral window of interest. The total amount of excited atom N_0 was increased until

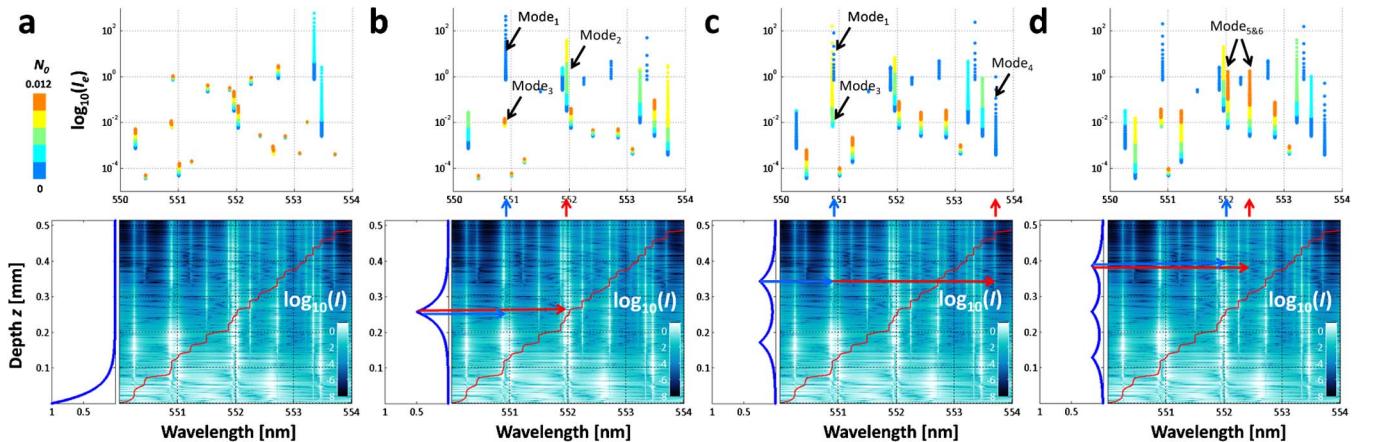


Fig. 4. Different excitation profiles $N_{\text{ex}}(z)$ with $h = 0$ (a), $h = 1$ (b), $h = 2$ (c), and $h = 3$ (d), as shown in the lower left curves. Emission intensity I_e on a logarithmic scale as a function of the total amount of excited atoms N_0 (first row). The colors of the dots match with N_0 . Field intensity $I(z)$ in the wavelength range of $\lambda = 550$ – 554 nm in the passive system with $N_0 = 0$ (second row).

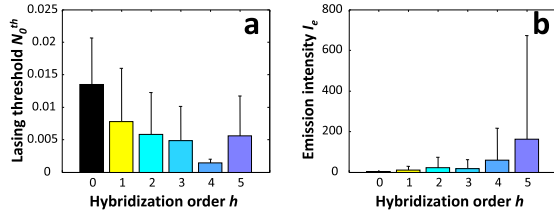


Fig. 5. (a) Averaged lasing threshold and (b) emission intensity I_e as a function of hybridization order h of the excitation field. The error bars are standard deviations.

a threshold of each mode N_0^{th} reached. In the excitation via the nonresonant mode, following an exponential decay in the shallow depth, most of the lasing modes were inert except for two modes in $\lambda = 553.4\text{--}553.5$ nm. When the gain profile is changed to the isolated localized mode [Fig. 4(b)], the number of activated lasing modes increased. The increased emission intensity and the decreased lasing threshold are clearly seen [first row of Fig. 4(b)]. Obviously, the spatial overlap between the excitation and emission field profiles [Mode 1 and Mode 2 as marked with the blue and red arrows in Fig. 4(b)] enhanced the lasing performance. Overall, although the lasing action can be enhanced by the excitation of the isolated localized modes, the overlapping area is still limited due to the relative narrow field width determined by ξ .

Figures 4(c) and 4(d) (left lower panels) shows the excitation via HLS ($h = 2$ and 3). When the second-order hybridized localized states were excited [Fig. 4(c)], the lasing in the weak emission modes was further enhanced. As shown in Mode 3, the emission intensity significantly increased within the N_0 range of interest. Similarly, the upper field of Mode 4 was overlapped by the excitation (red arrow), resulting in a low threshold $N_0^{\text{th}} = -6 \times 10^{-3}$, and achieved the same emission intensity with the isolated localized excitation. Mode 5 and Mode 6 were still inert in the case of the lower orders of HLS, because the gain regions were located near the end of the structure (blue and red arrows). However, these modes were easily activated with the excitation using the third-order hybridized localized state.

Finally, we quantified the lasing threshold and the emission intensity as a function of h of the excitation field. Figures 5(a) and 5(b) shows that the averaged lasing threshold decreases and the averaged emission intensity increases with h . Because the emission via HLS are more amplified than that of the isolated localized modes under the same amount of the stored energy,

the additional benefit is the enhanced emission intensity. We note that $h = 5$ is approximately a maximal order that can be formed in the current system [16]. Another interesting aspect of the lasing behavior of HLS is that modal interactions are not observed, although some lasing modes are very close spectrally [Fig. 4(d)]. Each hybridized state is confined due to suppression of modal interactions, supporting the idea that the current multimode lasing occurs in the Anderson localized regime [18].

In conclusion, the excitation light via HLS when $L \gg \xi$ can allow for the full utilization of deeply localized gain regions and could potentially be simple routes for overcoming some intrinsic limitations of random lasers. Our numerical studies will serve as a theoretical base for experiments using natural and biological multilayered nanostructures in optics.

This work was supported by the Samsung Global Research Outreach grant and the Korea Science and Engineering Foundation grant (NSF-2013R1A1A1A05011990).

References

1. J. B. Pendry, *J. Phys. C* **20**, 733 (1987).
2. A. V. Tartakovskii, M. V. Fistul, M. E. Raikh, and I. M. Ruzin, *Sov. Phys. Semicond.* **21**, 370 (1987).
3. J. Bertolotti, S. Gottardo, D. S. Wiersma, M. Ghulinyan, and L. Pavesi, *Phys. Rev. Lett.* **94**, 113903 (2005).
4. P. Sebbah, B. Hu, J. M. Klosner, and A. Z. Genack, *Phys. Rev. Lett.* **96**, 183902 (2006).
5. L. Chen and X. Y. Jiang, *J. Phys. Condens. Matter* **25**, 175901 (2013).
6. A. Pena, A. Girschik, F. Libisch, S. Rotter, and A. A. Chabanov, *Nat. Commun.* **5**, 3488 (2014).
7. S. H. Choi and Y. L. Kim, *Phys. Rev. B* **89**, 035115 (2014).
8. L. Labonte, C. Vanneste, and P. Sebbah, *Opt. Lett.* **37**, 1946 (2012).
9. V. Milner and A. Z. Genack, *Phys. Rev. Lett.* **94**, 073901 (2005).
10. A. L. Burin, M. A. Ratner, H. Cao, and S. H. Chang, *Phys. Rev. Lett.* **88**, 093904 (2002).
11. Y. Feng and K. Ueda, *Opt. Express* **12**, 3307 (2004).
12. T. M. Jordan, J. C. Partridge, and N. W. Roberts, *J. R. Soc. Interface* **11**, 20140948 (2014).
13. S. H. Choi, Y. L. Kim, and K. M. Byun, *Opt. Express* **18**, A458 (2010).
14. B. Payne, J. Andreasen, H. Cao, and A. Yamilov, *Phys. Rev. B* **82**, 104204 (2010).
15. Z. Shi, J. Wang, and A. Z. Genack, *Proc. Natl. Acad. Sci. USA* **111**, 2926 (2014).
16. J. Andreasen, C. Vanneste, L. Ge, and H. Cao, *Phys. Rev. A* **81**, 043818 (2010).
17. M. Ghulinyan, *Phys. Rev. A* **76**, 013822 (2007).
18. P. Stano and P. Jacquod, *Nat. Photonics* **7**, 66 (2013).